

Entanglement phases and phase transitions in monitored free fermion system due to localizations

Yu-Jun Zhao,^{1,2} Xuyang Huang,² Yi-Rui Zhang,² Han-Ze Li,^{2,3,*} and Jian-Xin Zhong^{2,1,†}

¹*School of Physics and Optoelectronics, Xiangtan University, Xiangtan 411105, China*

²*Institute for Quantum Science and Technology, Shanghai University, Shanghai 200444, China*

³*Department of Physics, National University of Singapore, Singapore 117542*

In recent years, the presence of local potentials has significantly enriched and diversified the entanglement patterns in monitored free fermion systems. In our approach, we employ the stochastic Schrödinger equation to simulate a one-dimensional spinless fermion system under continuous measurement and local potentials. By averaging the steady-state entanglement entropy over many quantum trajectories, we investigate its dependence on measurement and localization parameters. We used a phenomenological model to interpret the numerical results, and the results show that the introduction of local potentials does not destroy the universality class of the entanglement phase transition, and that the phase boundary is jointly characterized by the measurement process and the localization mechanism. This work offers a new perspective on the characterization of the entanglement phase boundary arising from the combined effects of measurement and localization, and provides criteria for detecting this novel phase transition in cold atom systems, trapped ions, and quantum dot arrays.

I. INTRODUCTION

Classical paradigms of nonequilibrium quantum physics—such as thermalization under the eigenstate thermalization hypothesis [1–5] and its counterpoint in the quantum Zeno effect [6–10], offer a striking tension: while coherent dynamics generically scramble information and build volume-law entanglement, frequent observations can freeze evolution by continually projecting local degrees of freedom. This tension naturally leads to the notion of a measurement-driven reorganization of quantum states: as the rate or strength of monitoring is increased, the balance between entanglement production and removal can qualitatively change, suggesting a sharp transition in the long-time entanglement structure. This phenomenon is now understood as a measurement-induced phase transition (MIPT), in which entanglement scaling morphs from volume law to area law due to the backaction of measurements.

A broad body of work has established both the ubiquity and diversity of MIPTs across platforms and protocols [11–59]. In random quantum circuits [29–43], interleaving unitary gates with stochastic measurements yields a finite-threshold transition. Related transitions appear under Hamiltonian dynamics with projective or continuous monitoring [44–48], and persist for both projective and weak measurements. Across these settings, the steady-state phases (volume, logarithmic/sub-volume, and area) and their critical properties depend on symmetries [12, 41, 52, 53], dimensionality [54], and the microscopic structure of measurements [30, 55–59], revealing a rich taxonomy of measurement-driven universality classes.

In the presence of localization, the landscape becomes more intricate. The root cause lies in the fact that localization tends to confine particles or quantum information to local regions, thereby significantly suppressing the generation and propagation of long-range entanglement. Different types of localization affect entanglement and information spreading through

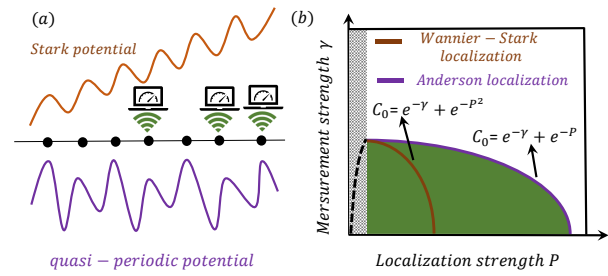


FIG. 1. (a): Monitored half-filled fermions in SP (brown) and QPP (purple). (b): The phase boundaries in the phase diagram are formed by different localization mechanisms (Wannier-Stark localization and Anderson localization). We present the general solution form, with specific parameters given below. The grey region corresponds to the case of a very weak localization potential, where we tend to revert to the results obtained from the Keldysh field theory [54]; the black dashed line corresponds to the phase boundary within this region.

their respective physical mechanisms, and may thus alter the stability of phases and critical behavior in different ways. For example, disorder or quasi-periodic potential(QPP) induced Anderson localization and Stark potential(SP) induced Stark localization imprint distinct single-particle spectra, spatial profiles and transport properties that can [60–81], in principle, reshape measurement-driven entanglement phases and transitions.

Against this backdrop, we ask two connected questions at the intersection of measurement and localization: (I) Will a change in the localization mechanism alter the critical universality class of the MIPT phase diagram, or do the two cases follow the same critical laws? (II) is it possible to formulate a unified understanding of entanglement phase transitions arising from the interplay between distinct localization mechanisms and measurements? Addressing these questions disentangles universal from non-universal ingredients in the measurement-localization competition and yields operational criteria for experimental tests across platforms ranging from

* hanzeli@u.nus.edu

† jxzhong@shu.edu.cn

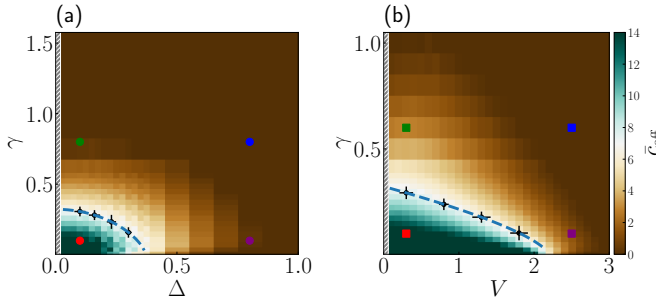


FIG. 2. Phase diagrams and phase boundaries extracted from the effective central charge. (a) Phase diagram under joint tuning of the measurement strength and SP strength; (b) Phase diagram under joint tuning of the measurement strength and the QPP strength. Colors indicate the effective central charge \bar{c}_{eff} , extracted from the finite-size scaling of half-chain entanglement entropy: green corresponds to large \bar{c}_{eff} values (log-law-like regime), while brown corresponds to $\bar{c}_{\text{eff}} \rightarrow 0$ (area-law regime). Dashed curves denote the semi-analytical expressions for phase boundaries derived by Eq. (11). Black solid dots mark four numerically fitted phase transition points and the grey region corresponds to the case of a very weak localization potential, where we tend to revert to the results obtained from the Keldysh field theory [54]; therefore, it is not shown in the diagram. In the subsequent finite-size scaling analysis, four representative points on each phase diagram (marked in red, green, blue, and purple, respectively) are selected to characterize the entanglement scaling behavior at the phase boundary of that point.

cold atomic systems [44–46, 82–84] and trapped ions [85, 86] to quantum dot arrays [87].

To address question (I), we employ a one-dimensional free-fermion system as our platform. Under both a SP (realizing Stark localization) and a QPP (realizing Anderson localization), we introduce random projective measurements with tunable strength. By analyzing the system's steady-state entanglement entropy and effective central charge, we investigate the impact of the measurement-localization coupling on the entanglement phase transition. For question (II), we identify the physical mechanisms that play a central role in the entanglement phase transition, thereby formulating a universal statement concerning different localization mechanisms. Furthermore, we obtain several physical pictures, which are summarized schematically in Fig. 1.

The remainder of this paper is organized as follows. In Sec. II, we introduce the tight-binding model in the presence of a localization potential and outline the quantum trajectory method used to simulate continuous measurement dynamics. In Sec. III, we present our understanding of the phase boundary arising from the interplay between different localization mechanisms and measurements, together with the entanglement phase diagram of MIPTs and the semi-analytical phase boundary we obtain. We then investigate the central charge, connected correlation function, and critical universality classes under both SP and QPP. Finally, Sec. IV summarizes the entire work.

II. MODEL AND METHOD

We consider a spinless one-dimensional fermions model with a localization, subject to continuous measurements:

$$H = -J \sum_j (c_j^\dagger c_{j+1} + \text{h.c.}) + \sum_j P_j n_j, \quad (1)$$

where c_j and c_j^\dagger are the annihilation and creation operators of the spinless fermion at site j , P_j represents the strength of potential at lattice site j . We initialize the system in a Néel state, that is, $\psi(t=0) = \prod_{i=1}^{L/2} c_{2i-1}^\dagger | \text{vac} \rangle$, where $|\text{vac}\rangle$ is the vacuum state, and consider its evolution under open boundary conditions (OBCs). We perform a quantum measurement uniformly for all sites with a finite measurement amplitude (frequency) γ :

$$d|\psi(t)\rangle = -iH|\psi(t)\rangle dt + \sum_{j=1}^L \left[\frac{c_j^\dagger c_j |\psi(t)\rangle}{\sqrt{\langle \psi(t) | n_j | \psi(t) \rangle}} - |\psi(t)\rangle \right] dW_j(t), \quad (2)$$

where $dW_j(t)$ takes 0 or 1 obeying the site-independent Poisson process, that is, $\langle \langle dW_j(t) \rangle \rangle = \gamma dt$. Here, $\langle \langle \dots \rangle \rangle$ is the average noise. As a result of the measurement process, there are many trajectories of wave functions starting from the fixed initial state. Hence, we need to take an average over many trajectories to examine the statistical properties of any observable. The main physical quantity that we address is entanglement entropy. Divide the system into two subsystems A and B , which have sizes ℓ and $L - \ell$ ($\ell \leq L/2$), respectively (L represents the system size). Then, the entanglement entropy is defined as:

$$S = -\text{Tr}(\rho_A \log \rho_A), \quad (3)$$

where ρ_A is the reduced density matrix of the subsystem A for a given wave function $|\psi\rangle$, that is, $\rho_A = \text{Tr}_B(|\psi\rangle\langle\psi|)$, where Tr_B is the partial trace with respect to the part B . S is initially 0 and increases over time, reaching a saturated value in the long-time limit. We calculate the long-time steady-state entanglement entropy for each trajectory, take their average, and finally obtain \bar{S} .

III. RESULTS

A. Phase boundaries

As stated in Sec. II, in the specific study, we divide the system into two subsystems, A and B , in order to calculate the entanglement entropy. Consider such a bipartite system governed by purely quantum dynamics, the growth rate of its entanglement entropy takes the following form [31, 88–91]:

$$\dot{S}_\ell = -i \|H_{AB}\| \lambda(\rho), \quad (4)$$

$$\lambda(\rho) := \text{Tr}(h_{AB} [\rho, \rho_A \otimes \mathbf{I}_B]), \quad (5)$$

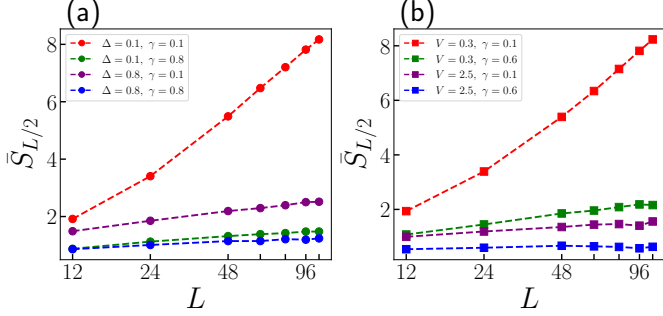


FIG. 3. Entanglement entropy versus system size for representative points. (a) Results corresponding to the four selected points from Fig. 1(a): $\Delta = 0.1, \gamma = 0.1$, $\Delta = 0.1, \gamma = 0.8$, $\Delta = 0.8, \gamma = 0.1$, and $\Delta = 0.8, \gamma = 0.8$; (b) Results corresponding to the four selected points from Fig. 1(b): $V = 0.3, \gamma = 0.1$, $V = 0.3, \gamma = 0.6$, $V = 2.5, \gamma = 0.1$, and $V = 2.5, \gamma = 0.6$. The plots show the half-chain entanglement entropy $\bar{S}_{L/2}$ as a function of system size L , revealing the scaling behavior under different potential and measurement strengths. Log-log axes are used throughout for visual clarity.

where $\rho = |\psi(t)\rangle\langle\psi(t)|$, $h_{AB} := H_{AB}/\|H_{AB}\|$ ($\|\dots\|$ is the operator norm), and \mathbf{I}_B is the identity operator for subsystem B . The Hamiltonian H_{AB} denotes the boundary interaction between subsystems A and B :

$$H_{AB} = \sum_{i \in A} \sum_{j \in B} h_{i,j}, \quad (6)$$

where $h_{i,j}$ is an interaction operator acting on sites i and j . Of interest is the case where $\ell = L/2$. In our study of a fermionic system without long-range interactions, the entanglement entropy growth rate is finite and takes a constant value, denoted as G_0 . Since measurements and local potentials both act to disentangle the system, even when small, the original volume-law entanglement entropy growth $S \sim G_0 t$ is transformed, under their combined effect, into a logarithmic form $S \sim \log(t)$, and, upon further increase, crosses over to an area-law scaling $S \sim t^0$. In our study, the phase boundary corresponds to the critical line separating the log-law region from the area-law region. Therefore, we find that at the phase boundary the entanglement entropy growth follows $S \sim C_0 \log(t)$, representing the lower bound of the log-law region and the upper bound of the area-law region (see Appendix A), where C_0 is a small constant. Assuming that under the influence of measurements and local potentials the initial entanglement growth rate is renormalized to $\Gamma(\gamma, P)G_0$, then at criticality one can write:

$$\Gamma(\gamma) + \Gamma(P) \sim C_0, \quad (7)$$

$\Gamma(\gamma)$ represents the entanglement suppression rate induced by the measurement strength γ . It quantifies the degree to which entanglement growth is suppressed per unit time under continuous measurement interventions. When γ is sufficiently large, entanglement growth can be strongly inhibited or even fully halted. To analyze this process quantitatively, we decom-

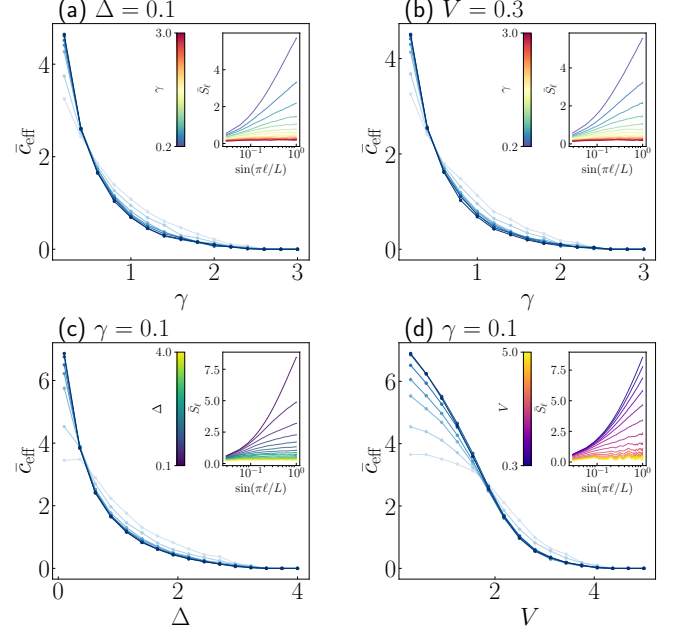


FIG. 4. Effective central charge \bar{c}_{eff} versus various control parameters with entanglement scaling insets. (a) Fixed $\Delta = 0.1$, varying measurement strength; (b) fixed $V = 0.3$, varying measurement strength; (c) fixed $\gamma = 0.1$, varying SP strength; (d) fixed $\gamma = 0.1$, varying QPP strength. Insets display entanglement entropy versus $\sin(\pi\ell/L)$ on a logarithmic x -axis to emphasize scaling behavior. Shades of blue from light to dark correspond to system sizes $L = 12, 24, 48, 64, 80, 96, 112$, the variation in system size is also reflected in the extent of the x -axis in the insets.

pose the system's evolution into individual quantum trajectories. Each trajectory corresponds to a specific measurement history, and the dynamics are governed by an effective non-Hermitian Hamiltonian:

$$H_{\text{eff}} = H - i \frac{\gamma}{2} \sum_u \mathcal{L}_u^\dagger \mathcal{L}_u, \quad (8)$$

where H is the original Hermitian Hamiltonian, γ is the measurement rate, and \mathcal{L}_u is the Lindblad operator. The non-Hermitian term captures the non-unitary dissipative effects introduced by measurements. Under this non-Hermitian evolution, Under the trajectory-weighted average, the initial entanglement-entropy growth rate of the system in the presence of measurements is renormalized to (please refer to Appendix A for details):

$$\Gamma(\gamma) \sim G_0 \exp(-\gamma). \quad (9)$$

As shown in Eq. (5), under purely unitary evolution, entanglement growth is driven by the boundary coupling between subsystems A and B . The entanglement growth rate is fundamentally determined by the Hamiltonian term H_{AB} that connects A and B . In the presence of a local potential, the spatial localization of particle states significantly suppresses the

boundary coupling between regions, leading to a pronounced reduction in the entanglement growth rate [92]. Corresponding to the distinct localization properties of the wave functions in the SP and the QPP systems, the entanglement growth rate is modified by the local potentials as:

$$\Gamma(P) \sim \begin{cases} G_0 \exp(-\Delta^2), & \text{SP} \\ G_0 \exp(-V), & \text{QPP} \end{cases} \quad (10)$$

where G_0 is the reference growth rate in the absence of any potential, Δ is the SP strength. Based on Eq. (7) and the envelope function of the entanglement growth rate Eq. (9) and Eq. (10), the phase boundaries in the systems with SP or QPP can be written as:

$$C_0 = \begin{cases} \exp(-6\gamma^{3/2}) + \exp(-8\Delta^2), & \text{SP} \\ \exp(-6\gamma^{3/2}) + \exp(-V/2). & \text{QPP} \end{cases} \quad (11)$$

To validate Eq. (11), we first map the effective central charge \bar{c}_{eff} over the parameter space spanned by the measurement strength γ and the local potential strength (either Stark, Δ , or quasi-periodic, V), thereby characterizing the scaling regimes of the entanglement entropy. As shown in Fig. 2, the phase diagrams under varying measurement and potential strengths are presented for the SP and QPP systems. The colormap encodes \bar{c}_{eff} extracted from half-chain entanglement entropy; the horizontal axis is the measurement rate γ , and the vertical axis is the potential strength Δ or V . The diagrams clearly separate area-law and log-law regimes: regions with large \bar{c}_{eff} correspond to log-law growth (an entanglement-spreading phase), whereas regions with $\bar{c}_{\text{eff}} \approx 0$ exhibit suppressed entanglement. We find that increasing either the SP or QPP shrinks the entangled region and eventually eliminates the phase boundary, although the deformation is qualitatively different between SP and QPP. The dashed curves are fits to Eq. (11), which agree closely with critical points obtained via finite-size scaling (black dots). As the potential strength increases, the entangled region narrows, the boundary bends, and eventually terminates, reflecting the progressively stronger suppression of entanglement propagation caused by localization. Importantly, the boundary deforms differently in the two cases: for SP, it changes super-exponentially with Δ^2 ; for QPP, it changes exponentially with V results that are fully consistent with the analytical structure established earlier. Together, they reveal a measurement-localization coupled entanglement phase transition: when the localization potential is small, the phase boundary is primarily determined by the measurement strength, and its descent is relatively gradual; as the localization potential increases, its suppression of entanglement growth causes the boundary to drop rapidly. However, because the Stark localization induced by SP is stronger than the Anderson localization induced by QPP, the phase boundary in Fig. 2(a) falls faster, reaching the area-law region much earlier.

To further verify the scaling characteristics of different regions, we examine the dependence of the entanglement entropy \bar{S} on the system size L , selecting representative points

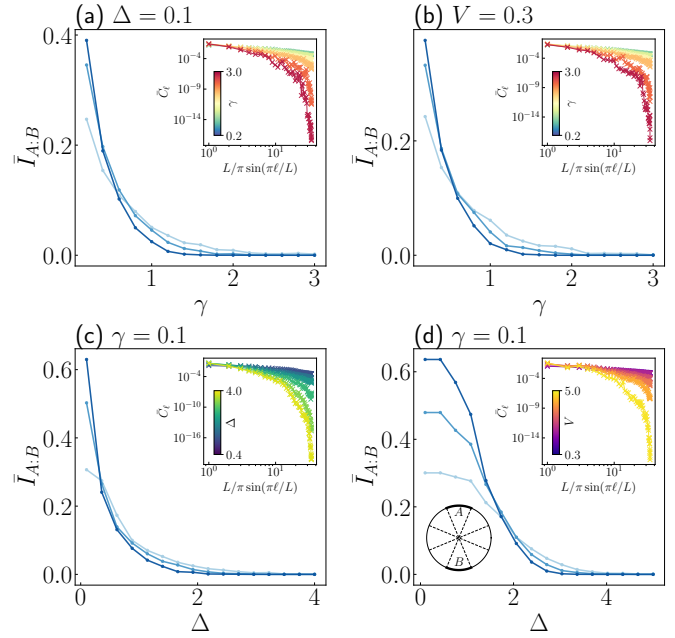


FIG. 5. Mutual information under varied control parameters, with scaling insets. (a) Fixed $\Delta = 0.1$, varying measurement strength γ ; (b) fixed potential strength $V = 0.3$, varying measurement strength γ ; (c) fixed measurement strength $\gamma = 0.1$, varying SP strength Δ ; (d) fixed $\gamma = 0.1$, varying QPP strength. Main panels show mutual information as a function of each parameter. Insets present correlation functions versus $\sin(\pi L/L)$, log-scaled on the x -axis to highlight scaling transitions. Shades of blue from light to dark correspond to system sizes $L = 12, 24, 48, 64, 80, 96, 112$, the variation in system size is also reflected in the extent of the x -axis in the insets.

(red, green, blue, purple) highlighted in Fig. 2. The corresponding results are shown in Fig. 3. It is evident that, under different measurement strengths and localization strengths, the dependence of \bar{S} on L exhibits significant differences. At the red-marked point in the phase diagram within the log-law region, \bar{S} shows a clear linear growth with $\log(L)$, indicating that the system is in a log-law-dominated phase. In this regime, the measurement rate and local potential are insufficient to significantly disrupt the propagation of particles or information across the entire system, leading to logarithmic growth of entanglement. In contrast, in the area-law region (i.e., at non-red points), \bar{S} rapidly saturates to a constant as $\log(L)$ increases. This reflects the fact that, under strong measurement or strong localization, the propagation of quantum information is strongly suppressed, and entanglement can only be established within a finite range near the boundaries between adjacent regions, without extending throughout the system. This transition from a log-law to an area-law scaling reflects a measurement-and-localization driven entanglement phase transition: when the measurement or localization strength crosses a critical value, the system's information propagation capability undergoes a sudden change, leading to an abrupt shift in the scaling behavior of the entanglement entropy and the emergence of a well-defined critical boundary.

B. Phases and phase transitions

We next follow the finite-size flow of the effective central charge \bar{c}_{eff} under OBCs. For each size L we fit the entanglement profile to Eq. (12) and obtain a single \bar{c}_{eff} subjected to different measurement intensities and local potentials, as illustrated in Fig. 4. Near criticality, the half-chain entanglement entropy exhibits logarithmic scaling consistent with non-unitary conformal field theory:

$$\bar{S}(\ell, L) = \frac{\bar{c}_{\text{eff}}}{3} \ln \left[\frac{L}{\pi} \sin \left(\frac{\pi \ell}{L} \right) \right] + s_0, \quad (12)$$

where ℓ is the subsystem size, \bar{c}_{eff} is the effective central charge, and s_0 is a non-universal constant. In the thermodynamic limit, $\bar{c}_{\text{eff}} \rightarrow 0$ in the area-law phase, while it remains finite in the logarithmic phase, thus serving as a diagnostic for the transition. As shown in Fig. 4(a,b), when the local potential is fixed at a small value ($\Delta = 0.1$ or $V = 0.3$), increasing the measurement strength γ causes \bar{c}_{eff} curves for different system sizes to gradually intersect, indicating a transition near $\gamma \approx 0.3$. The insets strongly corroborate this behavior: as γ increases, the entanglement entropy transitions from rapid growth to saturation, signaling a crossover from log-law to area-law scaling. Similarly, in Fig. 4(c,d), when the measurement strength is fixed at a low value ($\gamma = 0.1$), increasing the local potential strength leads to similar crossing behavior among different system sizes, with transition points occurring around $\Delta \approx 0.3$ and $V \approx 1.8$, respectively. The insets in Fig. 4 clearly demonstrate this effect: the entanglement entropy drops from steep growth to a nearly constant value as localization increases, again signifying a transition from log-law to area-law behavior. These results collectively indicate that both measurement strength and local potential can induce a phase transition in the system. In both cases, entanglement growth is suppressed, although the mechanisms and suppression profiles differ between SP and QPP. These observations reveal how both measurement and localization reduce boundary coupling and suppress entanglement growth. The distinct functional behaviors of SP and QPP reinforce the validity of \bar{c}_{eff} as a transition indicator.

Another independent indicator of the entanglement phase transition is the mutual information. As illustrated in Fig. 5(d), the system is partitioned into four segments: subsystems A and B , each occupying $L/8$ sites, are separated by two buffer regions of length $3L/8$. The mutual information is defined as

$$\bar{I}_{A:B} = \bar{S}_A + \bar{S}_B - \bar{S}_{AB}, \quad (13)$$

where \bar{S}_A , \bar{S}_B , and \bar{S}_{AB} denote the entanglement entropies of regions A , B , and $A \cup B$, respectively. Mutual information has proven to be a sensitive diagnostic of MIPT in a variety of systems [32, 46], due to its ability to capture nonlocal correlations. In our study, we adopt the same set of parameters used for computing \bar{c}_{eff} . As shown in Fig. 5(a,b), when the local potential is set to a small value ($\Delta = 0.1$ or $V = 0.3$), increasing the measurement strength γ leads to a crossing in mutual information curves across different system sizes, signaling the onset of a transition. Similarly, in Fig. 5(c,d), fixing

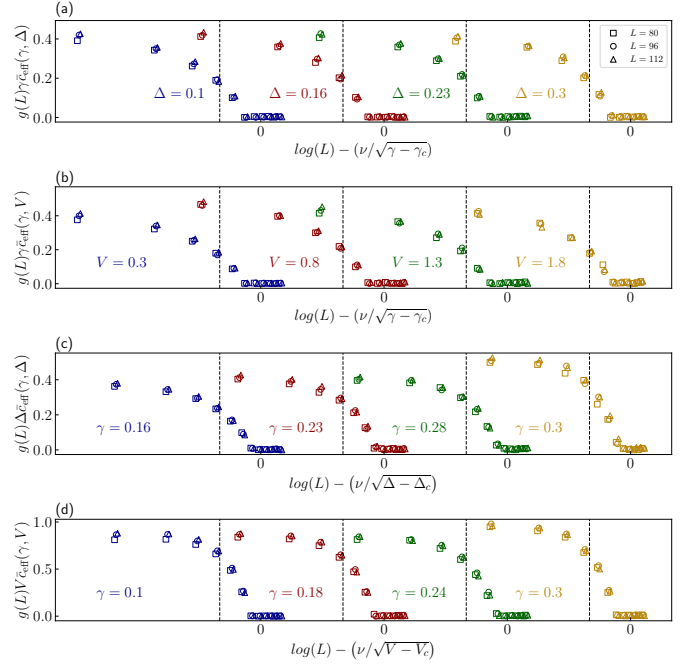


FIG. 6. Finite-size scaling for the effective central charge with the BKT scenario, (a): $g(L)\gamma\bar{c}_{\text{eff}}(\gamma, \Delta)$ versus $\log(L) - \nu/\sqrt{\gamma - \gamma_c}$, (b) : $g(L)\gamma\bar{c}_{\text{eff}}(\gamma, V)$ versus $\log L - \nu/\sqrt{\gamma - \gamma_c}$. (c): $g(L)\Delta\bar{c}_{\text{eff}}(\gamma, \Delta)$ versus $\log(L) - \nu/\sqrt{\Delta - \Delta_c}$, (d) : $g(L)V\bar{c}_{\text{eff}}(\gamma, V)$ versus $\log L - \nu/\sqrt{V - V_c}$. $g(L) = [1 + 1/(2 \log L - \alpha)]^{-1}$ Detailed numerical data are provided in Table. I.

the measurement strength and gradually increasing the potential strength (Δ or V) also induces such crossings, indicative of a phase boundary. To further understand the origin of these behaviors, we compute the connected correlation function defined as

$$\bar{C}_\ell = \langle \hat{n}_{L/2} \rangle \langle \hat{n}_{L/2+\ell} \rangle - \langle \hat{n}_{L/2} \hat{n}_{L/2+\ell} \rangle, \quad (14)$$

which reduces to $\bar{C}_\ell = |\langle \hat{c}_{L/2}^\dagger \hat{c}_{L/2+\ell} \rangle|^2$ for the Slater-determinant state $|\psi(t)\rangle$. As shown in the insets of Fig. 5, both increasing measurement strength and local potential lead to qualitatively similar changes in the correlation structure. In the low measurement or weak localization regime, \bar{C}_ℓ decays algebraically, $\bar{C}_\ell \sim \ell^{-\eta}$, indicating long-range correlations and rapid entanglement growth. In the strong measurement or deep localized regime, \bar{C}_ℓ decays exponentially, $\bar{C}_\ell \sim \exp(-\ell/\xi)$, suggesting short-range correlations and saturation of entanglement entropy consistent with area-law behavior. This sharp decay in the correlation function confirms a transition from an entangled phase with extended quantum coherence to a localized phase dominated by measurement or potential-induced suppression. Together with mutual information crossings, these results demonstrate that both measurement and disorder drive a phase transition that limits entanglement growth, with distinct suppression mechanisms depending on the type of local potential applied.

To quantitatively determine the location and nature of the entanglement phase transition, we perform a finite-

TABLE I. Data collapse parameters for the effective central charge results.

Data	Δ/V				$\gamma(\Delta)/\gamma(V)$			
	0.1/0.3	0.16/0.8	0.23/1.3	0.3/1.8	0.16/0.1	0.23/0.18	0.28/0.24	0.3/0.3
γ_c or Δ_c/V_c	0.3/0.3	0.28/0.24	0.23/0.18	0.16/0.1	0.1/0.3	0.16/0.8	0.23/1.3	0.3/1.8
ν	3.8/2.7	4.1/2.9	5.7/3.3	6.5/3.8	3.3/2.6	4.1/2.9	4.9/3.2	6.5/3.6
α	5.9/4.1	6.2/4.3	6.5/4.5	7.3/4.9	4.9/3.2	6.5/4.1	7.4/4.8	8.9/5.3

size scaling and data collapse analysis of the effective entanglement quantity \bar{c}_{eff} within the Berezinskii-Kosterlitz-Thouless (BKT) framework. Given the pronounced finite-size corrections in free-fermion circuits, simple visual identification of crossing points is unreliable. We adopt a single-parameter scaling ansatz with a mild size correction factor $g(L)$, incorporating the essential singularity of the BKT correlation length, expressed as $g(L) x \bar{c}_{\text{eff}}(x, y) = F[\log(L \xi(x, x_c(y)))]$, where $x \in \{\gamma, \Delta, V\}$ and $\xi(x, x_c) \sim \exp[-\nu/\sqrt{|x - x_c|}]$. This yields natural scaling variables $X_x = \log L - \nu/\sqrt{|x - x_c|}$ and $Y_x = g(L) x \bar{c}_{\text{eff}}$, allowing us to absorb leading finite-size drift and achieve data collapse onto a unified master curve across system sizes and parameter paths. Fig. 6 illustrates this systematic validation across multiple paths: (a) for fixed local potential $\Delta = (0.1, 0.16, 0.23, 0.3)$, data from system sizes $L = 80, 96, 112$ collapse well after rescaling, enabling precise determination of $\gamma_c(\Delta)$ and a shared ν ; (b) repeating the analysis for different potential strengths $V = \{0.3, 0.8, 1.3, 1.8\}$, we trace the evolution of $\gamma_c(V)$; (c) scanning Δ at fixed measurement strengths $\gamma = \{0.16, 0.23, 0.28, 0.30\}$, we extract $\Delta_c(\gamma)$, which agrees with the inverse function from (a); (d) scanning V at fixed $\gamma = \{0.10, 0.18, 0.24, 0.30\}$, we determine $V_c(\gamma)$, completing the critical boundary in the (γ, V) plane. The critical points obtained from all four paths are consistently described using a unified scaling function F and a common critical exponent ν , indicating that the local potential does not merely shift an isolated critical point but cooperates with measurement strength to generate a continuous phase boundary in the (γ, Δ, V) parameter space. Mathematically, while measurement tends to suppress entanglement, the local potential restructures the state and alters information transport, and the competition between these effects determines the geometry and location of the phase boundary governed by the BKT singularity. The successful data collapses validate the applicability and robustness of the BKT scaling framework and provide a quantitative foundation for extracting the critical points $\gamma_c(\Delta)$, $\gamma_c(V)$, $\Delta_c(\gamma)$, $V_c(\gamma)$, and the correlation length exponent ν .

IV. CONCLUSION AND DISCUSSION

We investigated the continuous measurement of free fermions under SP and QPP. Our study shows that when the SP strength or the measurement strength is weak, the system remains in a stable logarithmic-scaling phase. Moreover, we found that increasing either the measurement strength or

the SP triggers a phase transition, pushing the system into an area-law phase. When the potential strength is strong, we demonstrate that the MIPT disappears, and regardless of the measurement strength, the system remains stable in the area-law phase. To further support these results, we analyzed the central charge, mutual information, and correlation functions. The results reveal that using central charge and mutual information to characterize the system's entanglement behavior clearly exposes a crossover phenomenon, indicating that an increase in either measurement strength or SP leads to an entanglement phase transition. These findings suggest that, qualitatively, Stark localization (caused by SP) and Anderson localization (caused by QPP) play equivalent roles in driving entanglement phase transitions, and both belong to the BKT universality class.

Furthermore, we present an understanding of the entanglement phase transition under the combined influence of localization potential and measurement: the phase boundary is jointly determined by both factors and depends on the type of localization induced by the potential, rather than the potential itself.

Our work highlights the distinctive behavior of MIPTs and relaxation dynamics in Stark-driven monitored systems, offers a new perspective on the characterization of the entanglement phase boundary arising from the combined effects of measurement and localization.

ACKNOWLEDGMENTS

We thank Shuo Liu and Ze-Chuan Liu for the discussions. H.-Z. Li is supported by the CSC scholarship. J.-X. Zhong acknowledges the Shanghai University Distinguished Professor Research Start-up Project, the National Natural Science Foundation of China (Grant No.11874316 and No.12374046), the National Basic Research Program of China (Grant No.2015CB921103), and the Program for Changjiang Scholars and Innovative Research Team in University (Grant No.IRT13093).

Appendix A: Discussion on the Phase Boundary

As shown in Fig. 7, the entanglement entropy growth of the system exhibits distinct behaviors in different phases. From the figure, in the initial moment ($t \rightarrow 0$) within the Entangling phase the growth obeys:

$$S(t) = G_0 t, \quad (\text{A1})$$

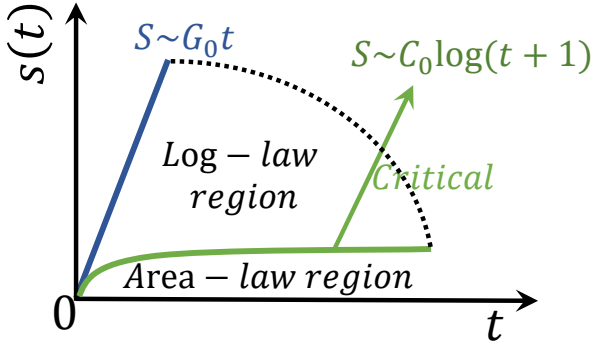


FIG. 7. The growth of bipartite entanglement entropy between the two semi-infinite halves of an infinite chain is shown. In the entangling phase (upper curve) the entanglement grows ballistically with time. At the critical point (middle curve), the entanglement grows logarithmically. In the disentangling phase (lower curve), the entanglement saturates to a finite value.

whereas under Critical dynamics it follows:

$$S(t) = C_0 \log(t + 1). \quad (\text{A2})$$

After introducing measurements or local potentials, the entanglement growth of the system is modified. Denoting the corrections due to measurements and local potentials by $\Gamma(\gamma)$ and $\Gamma(P)$, respectively, we have:

$$S(t) = \Gamma(\gamma)G_0t, S(t) = \Gamma(P)G_0t, \quad (\text{A3})$$

Hence, once measurements and local potentials suppress the Entangling-phase growth rate down to that of the critical phase, the system reaches criticality:

$$G_0\Gamma(\gamma) + G_0\Gamma(P) = C_0/(t + 1), \quad (\text{A4})$$

For the measurement-induced renormalization of the entanglement-growth rate $\Gamma(\gamma)$, We know that for a continuously monitored fermionic system, the dynamics is governed by the Lindblad master equation:

$$\begin{aligned} \frac{d\rho_t}{dt} &= \mathcal{L}\rho_t \\ &= -i\hat{H}_{\text{eff}}\rho_t + i\rho_t\hat{H}_{\text{eff}}^\dagger + \gamma \sum_m^{L-1} \hat{L}_m \rho_t \hat{L}_m^\dagger, \end{aligned} \quad (\text{A5})$$

where the non-Hermitian effective Hamiltonian H_{eff} is given by Eq. (5). In our actual calculations, we employ the Itô stochastic differential equation averaged over multiple trajectories,

so that any amplitude to propagate across L sites without a jump decays as:

$$p_{\text{surv}}(L, t) = e^{-\gamma L t}. \quad (\text{A6})$$

Meanwhile, the unitary Lieb-Robinson bound gives for the creation amplitude across distance L in time t :

$$A_0(L, t) \leq C_0 \exp\left(-\frac{L-v}{\xi_0} t\right). \quad (\text{A7})$$

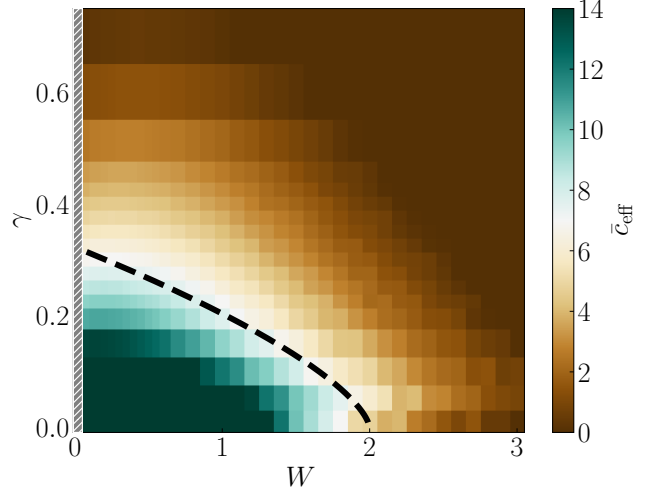


FIG. 8. Phase diagrams and phase boundaries extracted from the effective central charge under joint tuning of the measurement strength and Anderson disorder. Colors indicate the effective central charge \bar{c}_{eff} , extracted from the finite-size scaling of half-chain entanglement entropy: green corresponds to large \bar{c}_{eff} values (log-law-like regime), while brown corresponds to $\bar{c}_{\text{eff}} \rightarrow 0$ (area-law regime). The grey region corresponds to the case of a very weak localization potential, where we tend to revert to the results obtained from the Keldysh field theory [54]. Dashed curves denote the semi-analytical expressions for phase boundaries derived earlier.

Requiring both "no-jump" and unitary spread,

$$A(\gamma; L, t) \lesssim C_0 \exp\left(-\frac{L-vt}{\xi_0}\right) \exp(-\gamma L t). \quad (\text{A8})$$

A saddle-point optimization in (L, t) shows that the maximal amplitude obeys:

$$\max_{L, t} A(\gamma; L, t) \propto \exp(-a\gamma^b), \quad (\text{A9})$$

Since Γ is proportional to this amplitude scale, we set

$$\Gamma(\gamma) = \exp(-a\gamma^b), \quad (\text{A10})$$

this is the entanglement suppression rate induced by measurement. For the local potentials induced renormalization of the entanglement-growth rate $\Gamma(P)$, consider the single-particle tight-binding Hamiltonian as shown in Eq. (II), as an illustrative example, we choose the SP:

$$P_j = F_j, \quad (\text{A11})$$

$F_j = \Delta \cdot j/L$, where Δ denotes the maximum SP. Its eigenstates—the Wannier-Stark ladder-expand in the site basis as:

$$\psi_n(j) = J_{j-n}\left(\frac{2J}{\Delta}\right), \quad (\text{A12})$$

where $J_m(z)$ is the Bessel function. For large order $m \gg z$, one uses the asymptotic

$$J_m(z) \sim \exp\left(-m \ln \frac{2m}{e z} + O(\ln m)\right) \quad (\text{A13})$$

$$\approx \exp(-cm^d). \quad (\text{A14})$$

Setting $m \approx |j - n|$ and defining the localization length $\xi = 2J/\Delta$, the effective boundary coupling between regions A and B obeys

$$\|H_{AB}(\Delta)\| = \sum_{i \in A, j \in B} |J_{i-j}(2J/\Delta)| \quad (\text{A15})$$

$$\approx \|H_{AB}\| \exp(-c\Delta^d). \quad (\text{A16})$$

By the same Lieb-Robinson argument, the unitary entanglement growth rate is bounded by:

$$\Gamma(\Delta) \leq \|H_{AB}(\Delta)\|, \quad (\text{A17})$$

and we choose the tight form:

$$\Gamma(\Delta) = G_0 \exp[-c\Delta^d], \quad (\text{A18})$$

this is the entanglement entropy growth rate corrected by the SP. Similarly, for a one-dimensional QPP,

$$P_j = V \cos(2\pi\beta j + \varphi), \quad (\text{A19})$$

V is the strength of the QPP, the single-particle eigenfunctions localize exponentially with localization length $\xi(V)$. Hence the entanglement entropy growth rate is suppressed to

$$\Gamma(V) = G_0 \exp(-eV). \quad (\text{A20})$$

Then, the phase boundaries in the systems with SP or QPP can be written as:

$$C_0 = \begin{cases} \exp(-a\gamma^b) + \exp(-c\Delta^d), & \text{SP} \\ \exp(-a\gamma^b) + \exp(-eV), & \text{QPP} \end{cases} \quad (\text{A21})$$

Eq. (A21) is the general solution we finally obtain, and in this paper we fix the parameters as $(a, b, c, d, e, C_0) = (6, 1.5, 8, 2, 0.5, 3)$.

Appendix B: Free fermions with Anderson disorder under measurement

We here complement the results for the SP and QPP by presenting the phase diagram of a one-dimensional chain of free fermions subject to Anderson-type disorder and continuous measurement. We consider spinless free fermions on a one-dimensional lattice with nearest-neighbor hopping J in the presence of uncorrelated on-site disorder:

$$H = -J \sum_{i=1}^{L-1} (c_i^\dagger c_{i+1} + c_{i+1}^\dagger c_i) + \sum_{i=1}^L \varepsilon_i n_i, \quad (\text{B1})$$

where c_i^\dagger (c_i) creates (annihilates) a fermion at site i , and $n_i = c_i^\dagger c_i$ is the local number operator. The on-site potential ε_i is an independent random variable drawn from the uniform distribution $[-W, W]$, where W is the disorder strength. We set $J = 1$ as the unit of energy and impose the same boundary conditions and filling as in the main text. In the Fig. 8, strong measurement or strong disorder yields an area-law phase with $\bar{c}_{\text{eff}} \approx 0$, while weak measurement and weak disorder produce a logarithmic-entanglement phase with $\bar{c}_{\text{eff}} > 0$. The phase boundary predicted by Eq. (11) in the main text is determined by the competition between the measurement-induced disentangling rate and the effective propagation scale set by localization, and it agrees very well with the numerically obtained transition line. Using the same parameters as for the quasiperiodic potential, we achieve an accurate fit to the phase boundary in the disordered phase diagram. This further supports our conclusion that the phase boundary depends only on the localization characteristics of the wave function; that is, as long as the lattice potential leads to the same degree of localization, the phase boundaries will be similar, largely independent of the specific form of the potential used in the model.

-
- [1] J. M. Deutsch, Quantum statistical mechanics in a closed system, *Physical Review A* **43**, 2046 (1991).
- [2] M. Srednicki, Chaos and quantum thermalization, *Physical Review E* **50**, 888 (1994).
- [3] M. Rigol, V. Dunjko, and M. Olshanii, Thermalization and its mechanism for generic isolated quantum systems, *Nature* **452**, 854 (2008).
- [4] L. D'Alessio, Y. Kafri, A. Polkovnikov, and M. Rigol, From quantum chaos and eigenstate thermalization to statistical mechanics and thermodynamics, *Advances in Physics* **65**, 239 (2016).
- [5] H. Kim, T. N. Ikeda, and D. A. Huse, Testing whether all eigenstates obey the eigenstate thermalization hypothesis, *Physical Review E* **90**, 052105 (2014).
- [6] B. Misra and E. C. G. Sudarshan, The zeno's paradox in quantum theory, *Journal of Mathematical Physics* **18**, 756 (1977).
- [7] W. M. Itano, D. J. Heinzen, J. J. Bollinger, and D. J. Wineland, Quantum zeno effect, *Physical Review A* **41**, 2295 (1990).
- [8] P. Facchi and S. Pascazio, Quantum zeno subspaces, *Physical Review Letters* **89**, 080401 (2002).
- [9] A. G. Kofman and G. Kurizki, Acceleration of quantum decay processes by frequent observations, *Nature* **405**, 546 (2000).
- [10] P. Facchi, H. Nakazato, and S. Pascazio, From the quantum zeno to the inverse quantum zeno effect, *Physical Review Letters* **86**, 2699 (2001).
- [11] M. P. Fisher, V. Khemani, A. Nahum, and S. Vijay, Random quantum circuits, *Annual Review of Condensed Matter Physics* **14**, 335 (2023).
- [12] Y. Han and X. Chen, Measurement-induced criticality in \mathbb{Z}_2 -symmetric quantum automaton circuits, *Physical Review B* **105**, 064306 (2022).
- [13] X. Turkeshi, A. Biella, R. Fazio, M. Dalmonte, and M. Schirò, Measurement-induced entanglement transitions in the quantum Ising chain: From infinite to zero clicks, *Physical Review B* **103**, 224210 (2021).
- [14] P. Sierant, G. Chiriacò, F. Surace, S. Sharma, X. Turkeshi, M. Dalmonte, R. Fazio, and G. Pagano, Dissipative floquet dynamics: from steady state to measurement induced criticality in trapped-ion chains, *Quantum* **6**, 638 (2022).

- [15] P. Sierant and X. Turkeshi, Universal behavior beyond multifractality of wave functions at measurement-induced phase transitions, *Physical Review Letters* **128**, 130605 (2022).
- [16] S. Sharma, X. Turkeshi, R. Fazio, and M. Dalmonte, Measurement-induced criticality in extended and long-range unitary circuits, *SciPost Physics Core* **5**, 023 (2022).
- [17] X. Turkeshi, Measurement-induced criticality as a data-structure transition, *Physical Review B* **106**, 144313 (2022).
- [18] P. Sierant, M. Schirò, M. Lewenstein, and X. Turkeshi, Measurement-induced phase transitions in (d+1)-dimensional stabilizer circuits, *Physical Review B* **106**, 214316 (2022).
- [19] A. Paviglianiti, X. Turkeshi, M. Schirò, and A. Silva, Enhanced entanglement in the measurement-altered quantum ising chain, *Quantum* **8**, 1576 (2024).
- [20] B. Ladewig, S. Diehl, and M. Buchhold, Monitored open fermion dynamics: Exploring the interplay of measurement, decoherence, and free hamiltonian evolution, *Physical Review Research* **4**, 033001 (2022).
- [21] M. Buchhold, T. Müller, and S. Diehl, Revealing measurement-induced phase transitions by pre-selection, *arXiv preprint* (2022), 2208.10506.
- [22] T. Botzung, M. Buchhold, S. Diehl, and M. Müller, Robustness and measurement-induced percolation of the surface code, *arXiv preprint* (2023), 2311.14338.
- [23] W. Wang, S. Liu, J. Li, S. Zhang, and S. Yin, arxiv:2411.06648, *arXiv preprint* (2024), 2411.06648.
- [24] Z. Xiao, T. Ohtsuki, and K. Kawabata, arxiv:2408.16974, *arXiv preprint* (2025), 2408.16974.
- [25] T. Jin and D. Martin, Kardar-parisi-zhang physics and phase transition in a classical single random walker under continuous measurement, *Physical Review Letters* **129**, 260603 (2022).
- [26] T. Jin and D. Martin, Measurement-induced phase transition in a single-body tight-binding model, *Physical Review B* **110**, L060202 (2024).
- [27] G. Lee, T. Jin, Y. Wang, A. McDonald, and A. Clerk, Entanglement phase transition due to reciprocity breaking without measurement or postselection, *PRX Quantum* **5**, 010313 (2024).
- [28] M. Adani, S. Cavazzoni, B. Teklu, P. Bordone, and M. Paris, Measurement-induced entanglement phase transition in free fermion systems, *Scientific Reports* **14**, 19933 (2024).
- [29] Y. Li, X. Chen, and M. P. A. Fisher, Quantum zeno effect and the many-body entanglement transition, *Physical Review B* **98**, 205136 (2018).
- [30] A. Chan, R. M. Nandkishore, M. Pretko, and G. Smith, Unitary-projective entanglement dynamics, *Physical Review B* **99**, 224307 (2019).
- [31] B. Skinner, J. Ruhman, and A. Nahum, Measurement-induced phase transitions in the dynamics of entanglement, *Physical Review X* **9**, 031009 (2019).
- [32] Y. Li, X. Chen, and M. P. A. Fisher, Measurement-driven entanglement transition in hybrid quantum circuits, *Physical Review B* **100**, 134306 (2019).
- [33] M. J. Gullans and D. A. Huse, Dynamical purification phase transition induced by quantum measurements, *Physical Review X* **10**, 041020 (2020).
- [34] M. J. Gullans and D. A. Huse, Scalable probes of measurement-induced criticality, *Physical Review Letters* **125**, 070606 (2020).
- [35] C.-M. Jian, Y.-Z. You, R. Vasseur, and A. W. W. Ludwig, Measurement-induced criticality in random quantum circuits, *Physical Review B* **101**, 104302 (2020).
- [36] Y. Bao, S. Choi, and E. Altman, Theory of the phase transition in random unitary circuits with measurements, *Physical Review B* **101**, 104301 (2020).
- [37] S. Choi, Y. Bao, X.-L. Qi, and E. Altman, Quantum error correction in scrambling dynamics and measurement-induced phase transition, *Physical Review Letters* **125**, 030505 (2020).
- [38] M. Szyniszewski, A. Romito, and H. Schomerus, Entanglement transition from variable-strength weak measurements, *Physical Review B* **100**, 064204 (2019).
- [39] R. Fan, S. Vijay, A. Vishwanath, and Y.-Z. You, Self-organized error correction in random unitary circuits with measurement, *Physical Review B* **103**, 174309 (2021).
- [40] S. Vijay, Measurement-driven phase transition within a volume-law entangled phase, *arXiv preprint arXiv:2005.03052* (2020), arXiv:2005.03052 [quant-ph].
- [41] A. Lavasani, Y. Alavirad, and M. Barkeshli, Measurement-induced topological entanglement transitions in symmetric random quantum circuits, *Nature Physics* **17**, 342 (2021).
- [42] S. Sang and T. H. Hsieh, Measurement-protected quantum phases, *Physical Review Research* **3**, 023200 (2021).
- [43] M. Ippoliti, M. J. Gullans, S. Gopalakrishnan, D. A. Huse, and V. Khemani, Entanglement phase transitions in measurement-only dynamics, *Physical Review X* **11**, 011030 (2021).
- [44] Q. Tang and W. Zhu, Measurement-induced phase transition: A case study in the nonintegrable model by density-matrix renormalization group calculations, *Physical Review Research* **2**, 013022 (2020).
- [45] S. Goto and I. Danshita, Measurement-induced transitions of the entanglement scaling law in ultracold gases with controllable dissipation, *Physical Review A* **102**, 033316 (2020).
- [46] Y. Fuji and Y. Ashida, Measurement-induced quantum criticality under continuous monitoring, *Physical Review B* **102**, 054302 (2020).
- [47] D. Rossini and E. Vicari, Measurement-induced dynamics of many-body systems at quantum criticality, *Physical Review B* **102**, 035119 (2020).
- [48] O. Lunt and A. Pal, Measurement-induced entanglement transitions in many-body localized systems, *Physical Review Research* **2**, 043072 (2020).
- [49] M. Szyniszewski, O. Lunt, and A. Pal, Disordered monitored free fermions, *Phys. Rev. B* **108**, 165126 (2023).
- [50] T. Matsubara, K. Yamamoto, and A. Koga, Measurement-induced phase transitions for free fermions in a quasiperiodic potential, *Phys. Rev. B* **112**, 054309 (2025).
- [51] A. Lavasani, Y. Alavirad, and M. Barkeshli, Measurement-induced topological entanglement transitions in symmetric random quantum circuits, *Nature Physics* **17**, 342 (2021).
- [52] U. Agrawal, A. Zabalo, K. Chen, J. H. Wilson, A. C. Potter, J. H. Pixley, S. Gopalakrishnan, and R. Vasseur, Entanglement and charge-sharpening transitions in U(1) symmetric monitored quantum circuits, *Physical Review X* **12**, 041002 (2022).
- [53] F. Barratt, U. Agrawal, S. Gopalakrishnan, D. A. Huse, R. Vasseur, and A. C. Potter, Field theory of charge sharpening in symmetric monitored quantum circuits, *Physical Review Letters* **129**, 120604 (2022).
- [54] I. Pohoiko, P. Pöpperl, I. V. Gornyi, and A. D. Mirlin, Theory of free fermions under random projective measurements, *Phys. Rev. X* **13**, 041046 (2023).
- [55] N. Lang and H. P. Büchler, Entanglement transition in the projective transverse field ising model, *Physical Review B* **102**, 094204 (2020).
- [56] M. Coppola, E. Tirrito, D. Karevski, and M. Collura, Growth of entanglement entropy under local projective measurements, *Physical Review B* **105**, 094303 (2022).
- [57] M. Szyniszewski, A. Romito, and H. Schomerus, Universality of entanglement transitions from stroboscopic to continuous measurements, *Physical Review Letters* **125**, 210602 (2020).

- [58] G. De Tomasi and I. M. Khaymovich, Stable many-body localization under random continuous measurements in the no-click limit, *Physical Review B* **109**, 174205 (2024).
- [59] Q. Yang, Y. Zuo, and D. E. Liu, Keldysh nonlinear sigma model for a free-fermion gas under continuous measurements, *Physical Review Research* **5**, 033174 (2023).
- [60] P. W. Anderson, Absence of diffusion in certain random lattices, *Physical Review* **109**, 1492 (1958).
- [61] D. J. Thouless, A relation between the density of states and range of localization for one dimensional random systems, *Journal of Physics C: Solid State Physics* **5**, 77 (1972).
- [62] E. Abrahams, P. W. Anderson, D. C. Licciardello, and T. V. Ramakrishnan, Scaling theory of localization: Absence of quantum diffusion in two dimensions, *Physical Review Letters* **42**, 673 (1979).
- [63] G. H. Wannier, Wave functions and effective hamiltonian for bloch electrons in an electric field, *Physical Review* **117**, 432 (1960).
- [64] M. Glück, A. R. Kolovsky, and H. J. Korsch, Wannier–stark resonances in optical and semiconductor superlattices, *Physics Reports* **366**, 103 (2002).
- [65] J. X. Zhong and R. Mosseri, Quantum dynamics in quasiperiodic systems, *Journal of Physics: Condensed Matter* **7**, 8383 (1995).
- [66] J. Zhong, R. B. Diener, D. A. Steck, W. H. Oskay, M. G. Raizen, E. W. Plummer, Z. Zhang, and Q. Niu, Shape of the quantum diffusion front, *Physical Review Letters* **86**, 2485 (2001).
- [67] D. N. Maksimov, E. N. Bulgakov, and A. R. Kolovsky, Wannier–stark states in double-periodic lattices. i. one-dimensional lattices, *Physical Review A* **91**, 053631 (2015).
- [68] S. Longhi, Bloch oscillations in complex crystals with pt symmetry, *Physical Review Letters* **103**, 123601 (2009).
- [69] L. Bürkle, F. Fuchs, E. Ahlswede, W. Pletschen, and J. Schmitz, Wannier–stark localization in inas/(gain)sb superlattice diodes, *Physical Review B* **64**, 045315 (2001).
- [70] T. Hartmann, F. Keck, H. J. Korsch, and S. Mossmann, Dynamics of bloch oscillations, *New Journal of Physics* **6**, 2 (2004).
- [71] H. Z. Li, M. Wan, and J. X. Zhong, Fate of non-hermitian free fermions with wannier–stark ladder, *Physical Review B* **110**, 094310 (2024).
- [72] Y. J. Zhao, H. Z. Li, X. Huang, S. Z. Li, and J. X. Zhong, Fate of pseudomobility edges and multiple states in a non-hermitian wannier–stark lattice, *Physical Review B* **111**, 014315 (2025).
- [73] X. Huang, H. Z. Li, Y. J. Zhao, S. Liu, and J. X. Zhong, Quantum feedback induced entanglement relaxation and dynamical phase transition in monitored free fermion chains with a wannier–stark ladder, *Physical Review B* **111**, 184302 (2025).
- [74] J. E. Lye, L. Fallani, C. Fort, V. Guarnera, M. Modugno, D. S. Wiersma, and M. Inguscio, Effect of interactions on the localization of a bose-einstein condensate in a quasiperiodic lattice, *Physical Review A* **75**, 061603 (2007).
- [75] G. Roati, C. D’Errico, L. Fallani, M. Fattori, C. Fort, M. Zaccanti, G. Modugno, M. Modugno, and M. Inguscio, Anderson localization of a non-interacting bose–einstein condensate, *Nature* **453**, 895 (2008).
- [76] C. D’Errico, E. Lucioni, L. Tanzi, L. Gori, G. Roux, I. P. McCulloch, T. Giannarchi, M. Inguscio, and G. Modugno, Observation of a disordered bosonic insulator from weak to strong interactions, *Physical Review Letters* **113**, 095301 (2014).
- [77] M. Schreiber, S. S. Hodgman, P. Bordia, H. P. Lüschen, M. H. Fischer, R. Vosk, E. Altman, U. Schneider, and I. Bloch, Observation of many-body localization of interacting fermions in a quasirandom optical lattice, *Science* **349**, 842 (2015).
- [78] P. Bordia, H. Lüschen, S. Scherg, S. Gopalakrishnan, M. Knap, U. Schneider, and I. Bloch, Probing slow relaxation and many-body localization in two-dimensional quasiperiodic systems, *Physical Review X* **7**, 041047 (2017).
- [79] F. A. An, K. Padavić, E. J. Meier, S. Hegde, S. Ganeshan, J. H. Pixley, S. Vishveshwara, and B. Gadway, Interactions and mobility edges: Observing the generalized aubry-andré model, *Physical Review Letters* **126**, 040603 (2021).
- [80] P. G. Harper, Single band motion of conduction electrons in a uniform magnetic field, *Proceedings of the Physical Society. Section A* **68**, 874 (1955).
- [81] S. Aubry and G. André, Analyticity breaking and anderson localization in incommensurate lattices, *Annals of the Israel Physical Society* **3**, 18 (1980).
- [82] T. A. Corcovilos and J. Mittal, Two-dimensional optical quasicrystal potentials for ultracold atom experiments, *Applied Optics* **58**, 2256 (2019).
- [83] S. Diehl, A. Micheli, A. Kantian, B. Kraus, H. P. Büchler, and P. Zoller, Quantum states and phases in driven open quantum systems with cold atoms, *Nature Physics* **4**, 878 (2008).
- [84] O. Alberton, M. Buchhold, and S. Diehl, Entanglement transition in a monitored free-fermion chain: From extended criticality to area law, *Physical Review Letters* **126**, 170602 (2021).
- [85] C. Noel, P. Niroula, D. Zhu, A. Risinger, L. Egan, D. Biswas, M. Cetina, A. V. Gorshkov, M. J. Gullans, D. A. Huse, and C. Monroe, Measurement-induced quantum phases realized in a trapped-ion quantum computer, *Nature Physics* **18**, 760 (2022).
- [86] U. Agrawal, J. Lopez-Piqueres, R. Vasseur, S. Gopalakrishnan, and A. C. Potter, Observing quantum measurement collapse as a learnability phase transition, *Physical Review X* **14**, 041012 (2024).
- [87] C. W. Kim, J. M. Nichol, A. N. Jordan, and I. Franco, Analog quantum simulation of the dynamics of open quantum systems with quantum dots and microelectronic circuits, *PRX Quantum* **3**, 040308 (2022).
- [88] K. Van Acocleyen, M. Mariën, and F. Verstraete, Entanglement rates and area laws, *Physical Review Letters* **111**, 170501 (2013).
- [89] C. H. Bennett, A. W. Harrow, D. W. Leung, and J. A. Smolin, On the capacities of bipartite hamiltonians and unitary gates, *IEEE Transactions on Information Theory* **49**, 1895 (2003).
- [90] S. Bravyi, Upper bounds on entangling rates of bipartite hamiltonians, *Physical Review A* **76**, 052319 (2007).
- [91] T. Minato, K. Sugimoto, T. Kuwahara, and K. Saito, Fate of measurement-induced phase transition in long-range interactions, *Physical Review Letters* **128**, 010603 (2022).
- [92] J. H. Bardarson, F. Pollmann, and J. E. Moore, Unbounded growth of entanglement in models of many-body localization, *Physical Review Letters* **109**, 017202 (2012).